Molecular determinants of the mechanism and substrate specificity of *Clostridium difficile* proline-proline endopeptidase-1

Received for publication, April 23, 2019, and in revised form, May 27, 2019 Published, Papers in Press, June 10, 2019, DOI 10.1074/jbc.RA119.009029

Christian Pichlo[‡], Linda Juetten[§], Fabian Wojtalla[‡], Magdalena Schacherl[‡1], Dolores Diaz[§], and Ulrich Baumann[‡2]

From the [‡]Department of Chemistry, Institute of Biochemistry, University of Cologne, 50674 Cologne, Germany and [§]Department of Chemistry, Institute of Organic Chemistry, University of Cologne, 50939 Cologne, Germany

Edited by Ursula Jakob

Pro-Pro endopeptidase-1 (PPEP-1) is a secreted metalloprotease from the bacterial pathogen *Clostridium difficile* that cleaves two endogenous adhesion proteins. PPEP-1 is therefore important for bacterial motility and hence for efficient gut colonization during infection. PPEP-1 exhibits a unique specificity for Pro-Pro peptide bonds within the consensus sequence VNP ↓ PVP. In this study, we combined information from crystal and NMR structures with mutagenesis and enzyme kinetics to investigate the mechanism and substrate specificity of PPEP-1. Our analyses revealed that the substrate-binding cleft of PPEP-1 is shaped complementarily to the major conformation of the substrate in solution. We found that it possesses features that accept a tertiary amide and help discriminate P1′ residues by their amide hydrogen bond-donating potential. We also noted that residues Lys-101, Trp-103, and Glu-184 are crucial for proteolytic activity. Upon substrate binding, these residues position a flexible loop over the substrate-binding cleft and modulate the second coordination sphere of the catalytic zinc ion. On the basis of these findings, we propose an induced-fit model in which prestructured substrates are recognized followed by substrate positioning within the active-site cleft and a concomitant increase in the Lewis acidity of the catalytic Zn^{2+} ion. In conclusion, our findings provide detailed structural and mechanistic insights into the substrate recognition and specificity of PPEP-1 from the common gut pathogen *C. difficile*.

PPEP-1[3] (CD2830) is a highly specific, 24-kDa zinc metalloprotease secreted by *Clostridium difficile*, which cleaves substrates between two proline residues (1, 2). The expression levels of PPEP-1 and its endogenous substrates CD2831 and CD3246 depend inversely on the concentration of the second messenger cyclic di-GMP: PPEP-1 expression is up-regulated by low cyclic di-GMP concentrations via a c-di-GMP-I riboswitch, whereas the expression of CD2831 has been shown to be up regulated at high concentrations via a c-di-GMP-II riboswitch (3, 4). CD2831 is a cell wall–anchored adhesion protein that binds to collagen (5), whereas CD3246 is an as yet uncharacterized putative adhesion protein with a possible function in mediating host binding (6, 7). PPEP-1 releases its substrates from the cell surface by catalyzing the hydrolysis of peptide bonds in CD2831 and CD3246 within their C-terminal regions, which are linked to the peptidoglycan peptide stem. Consequently, deletion of PPEP-1 leads to an increased affinity of *C. difficile* to collagen type I as well as to an attenuated virulence in a hamster infection model (8), which directly links PPEP-1 function to the pathogenesis of *C. difficile*. It is thought that PPEP-1 is mainly involved in the regulation of the balance between attachment and detachment of *C. difficile* from the epithelial surface by cleaving CD2831 and CD3246. This process enables a more efficient dissemination of bacteria within the colon, thus leading to a more efficient gut colonization.

PPEP-1 was independently identified twice by different secretome analyses of *C. difficile* (1, 2). Investigation of its specificity yielded a consensus cleavage motif VNP ↓ PVP, revealing a strong preference of PPEP-1 toward proline residues at the positions P1, P1′, and P3′ (nomenclature according to Schechter and Berger (9)), although alanine is also accepted as a P1 or P1′ residue. Furthermore, PPEP-1 requires an asparagine residue at position P2 for efficient cleavage. The PPEP-1 substrates CD2831 and CD3246 contain clusters with multiple consecutive cleavage sites at their C termini (2). PPEP-1 was also found to hydrolyze certain model substrates at noncanonical sites, *e.g.* fibrinogen β (SLRP ↓ APP) (1), Hsp90 (PNA ↓ AVP), and IgA2 (PVP ↓ PPP) (2).

The crystal structure of PPEP-1 revealed a gluzincin metallopeptidase that showed a high degree of similarity to the peptidase domain of the anthrax lethal factor (LF) endopeptidase even though the sequence identity between both proteins was found to be low (21%) (Fig. 1) (10). A crystal structure of the inactive double mutant PPEP-1(E143A/Y178F) bound to a substrate peptide showed that PPEP-1 binds its substrate in a

The authors declare that they have no conflicts of interest with the contents of this article.

The atomic coordinates and structure factors (codes 6R4W, 6R4X, 6R4Y, 6R4Z, 6R5A, 6R5B, 6R5C, 6R9Z, 6R50, 6R51, 6R52, 6R53, 6R54, 6R55, 6R56, 6R57, 6R58, and 6R59) have been deposited in the Protein Data Bank (http://wwpdb.org/).

The NMR chemical shift data of this paper are available from the Biological Magnetic Resonance Data Bank under BMRB accession numbers 27862, 27863, and 27864.

This article contains Figs. S1–S11 and Tables S1–S12.

[1] Present address: Charité-Universitätsmedizin Berlin, Institute of Medical Physics and Biophysics, Charitéplatz 1,10117 Berlin, Germany.

[2] To whom correspondence should be addressed. Tel.: 49-221-470-3208; Fax: 49-221-470-5066; E-mail: ubaumann@uni-koeln.de.

[3] The abbreviations used are: (r)PPEP-1, (recombinant) Pro-Pro endopeptidase-1; LF, lethal factor; NTS/CTS, N-terminal/C-terminal subdomain; c-di-GMP, cyclic di-GMP; Abz, *ortho*-aminobenzoic acid; Dnp, 2,4-dinitrophenyl; r.m.s.d., root mean square deviation; PDB, Protein Data Bank; KEEN, Lys-101, Glu-184, Glu-185, Asn-3*; Fib, fibrinogen; pep, peptide; HBS, Hepes-buffered saline; DSS, 2,2-dimethyl-2-silapentane-5-sulfonic acid.

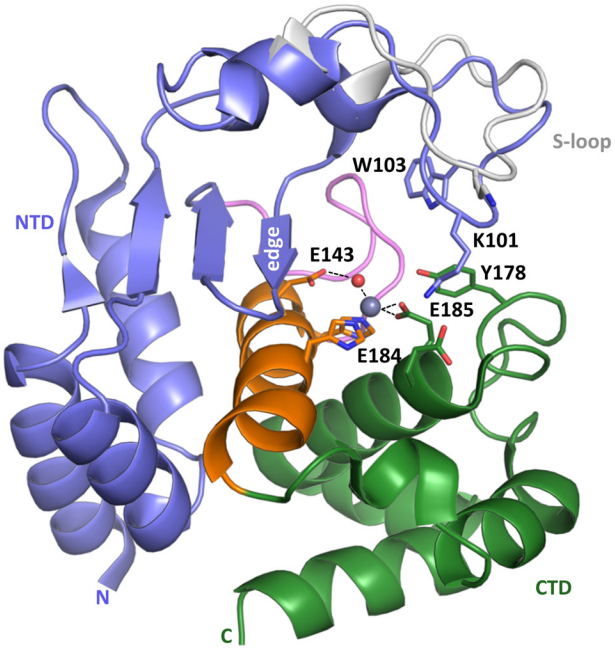

Figure 1. Ribbon diagram of PPEP-1. The active-site helix with the HE*XX*H motif is colored *orange*, the N-terminal subdomain (*NTD*) is in *blue*, and the C-terminal subdomain (*CTD*) is in *green*. The diverting loop is colored *magenta*. The S-loop is depicted in closed (*blue*) and open *gray*) conformations. The zinc ion is shown as a *gray sphere* together with a coordinating water molecule (*red*). The figure was prepared using PyMOL (38) and PDB code 5A0P.

unique double-kinked manner. The first kink is at position P1′, whereas the second kink occurs at P2′. This unusual double-kinked conformation is dictated by a unique loop of PPEP-1, called the diverting loop.

Another unusual structural feature of PPEP-1 is the so-called S-loop, which is located above the substrate-binding groove (Fig. 1). An NMR structure (11) of PPEP-1 as well as different crystal structures (10) showed that this loop undergoes conformational changes upon substrate binding and interacts at several positions with the substrate peptide. It was shown that it is a critical structural element required for proteolytic activity (11). In the substrate- and product-bound states, the S-loop is in a "closed" conformation. Together with other structural features such as the edge strand, the active-site helix, the diverting loop, and the gluzincin-specific helix carrying the third zinc ligand Glu-185, the S-loop forms a narrow hydrophobic tunnel around the substrate peptide at positions P1–P1′ (Fig. 1). This architecture explains why PPEP-1 accepts only small aliphatic amino acids there.

To uncover the exact underlying molecular reasons for the unique specificity of PPEP-1 and its catalytic determinants, we investigated its substrate-binding and hydrolysis mechanism in more detail using structural information and enzyme kinetics. We describe the importance of the S-loop for proteolytic activity, providing evidence for its dual role in substrate binding and catalysis. We also investigated the preference of PPEP-1 for prolines at positions P1 and P1′ and explained the specificity of PPEP-1 at position P1′.

Results

PPEP-1 prefers proline residues at P1′

For the determination of kinetic parameters, we established a steady-state kinetic assay using a set of internally quenched fluorogenic peptides (Table 1) containing the natural consensus recognition sequence of PPEP-1 derived from the cleavage sites in CD2831/CD3246 (VVN*X* ↓ *X*′VPPS). Depending on the peptide, positions P1 (*X*) and P1′ (*X*′) were filled with an alanine or proline residue. These peptides will be denoted from hereafter by their P1 and P1′ residues, *e.g.* Abz-AP-Dnp for the internally quenched fluorogenic peptide Abz-DVVNAPVPPSK-(Dnp)DD peptide (Table 1). Shorter and nonfluorescently labeled peptides used for crystallization are denoted in the same way, *e.g.* AP-pep for Ac-VVNAPVPP-$CONH_2$ (Table 2).

Correction of the raw data for inner-filter effects (12) enabled a quantitative evaluation of the fluorescence signal (Fig. S1). Because the "*trans*" conformation of the proline residues is required for cleavage by PPEP-1, conformational homogeneity of the different substrate peptides is crucial. To ensure no significant differences in the substrates because of variations in the *cis*/*trans* isomer of proline residues, we analyzed the substrate peptides via NMR. We observed different conformers for all peptides. In the case of the peptide Abz-AP-Dnp, the major conformer with all *X*-Pro peptide bonds in the *trans* conformation accounted for 92% of all species. For peptides Abz-PP-Dnp and Abz-AP-Dnp, we could not reliably quantify the ratio between the different conformers because of overlapping signals (Figs. S2–S4). Therefore, we analyzed the shorter peptides PP-pep, AP-pep, and PA-pep (Table 2). Approximately 85% of each peptide occurred in the "all-*trans*" conformation (Table S1–S3), confirming that Ala/Pro substitutions have no significant impact on the ratio of *cis*/*trans* conformations.

PPEP-1 had a K_m value of 137 μM and a k_{cat} value of 4.3 s^{-1} for the substrate Abz-PP-Dnp (Fig. 2*A*). In comparison, the K_m value for Abz-AP-Dnp was 43.6 μM, and the k_{cat} was 1.26 s^{-1}. As a result, the catalytic efficiency, k_{cat}/K_m, toward Abz-PP-Dnp and Abz-AP-Dnp was almost identical, 30,000 M^{-1} s^{-1} (Fig. 2*A*). In contrast, for Abz-PA-Dnp the K_m of PPEP-1 was 82.5 μM with a k_{cat} value of 0.87 s^{-1}. Thus, the resulting catalytic efficiency of about 10,000 M^{-1} s^{-1} was 3-fold lower compared with Abz-PP-Dnp, showing that PPEP-1 was more selective for a proline residue at position P1′. Interestingly, although the K_m value was only slightly reduced compared with the parent Abz-PP-Dnp, the turnover number, k_{cat}, was severely diminished.

Structural investigation of the proline-proline peptide bond specificity

To identify the structural basis of the observed kinetic differences, the structures of the inactive double mutant PPEP-1(E143A/Y178F) cocrystallized with peptides PA-pep and AP-pep (Table 2) were determined at 1.90 and 1.39 Å resolution, respectively (Table S4). The peptides PA-pep and AP-pep were well-defined in the electron density maps. However, no electron density was found at the expected position of the Zn^{2+} ion, revealing that the protein was unintentionally cocrystallized in its apo form (*i.e.* without Zn^{2+}). The conformations of

Table 1
Sequences of Abz/Dnp internally quenched fluorogenic peptides
N, N terminus; P5–P8′, assumed residue position in the substrate-binding cleft of PPEP-1 according to Schechter and Berger (9); C, C terminus; Lys* = *N*ϵ-(2,4-dinitrophenyl)-L-lysine; $CONH_2$, amidated C terminus; AA, amino acid.

	Position														
Name	N	5	4	3	2	1	1′	2′	3′	4′	5′	6′	7′	8′	C
Abz-PP-Dnp	Abz	Asp	Val	Val	Asn	Pro	Pro	Val	Pro	Pro	Ser	Lys*	Asp	Asp	$CONH_2$
Abz-PA-Dnp	Abz	Asp	Val	Val	Asn	Pro	Ala	Val	Pro	Pro	Ser	Lys*	Asp	Asp	$CONH_2$
Abz-AP-Dnp	Abz	Asp	Val	Val	Asn	Ala	Pro	Val	Pro	Pro	Ser	Lys*	Asp	Asp	$CONH_2$
AA position		1	2	3	4	5	6	7	8	9	10	11	12	13	

Table 2
Sequences of peptides used for cocrystallization
N, acetylated N terminus; P4–P3′, residue position in the substrate-binding cleft of PPEP-1 according to Schechter and Berger (9); C, C terminus; $CONH_2$, amidated C terminus; AA, amino acid.

	Position								
Name	N	P4	P3	P2	P1	P1′	P2′	P3′	C
PP-pep	Ac	Glu	Val	Asn	Pro	Pro	Val	Pro	$CONH_2$
PA-pep	Ac	Glu	Val	Asn	Pro	Ala	Val	Pro	$CONH_2$
AP-pep	Ac	Glu	Val	Asn	Ala	Pro	Val	Pro	$CONH_2$
APP-pep	Ac	Glu	Val	Ala	Pro	Pro	Val	Pro	$CONH_2$
AA position		1	2	3	4	5	6	7	

AP-pep and PA-pep were found to be very similar to that of PP-pep (Fig. 2*B*).

The two kinks described earlier for PP-pep were also observed for PA-pep. However, at the scissile bond and at the primed sites the positioning of the substrate peptide was different. Although the backbone torsion angles Φ (−63°) und Ψ (+160°) of the P1′ alanine residue in PA-pep could also be adopted by a proline (13), the newly introduced NH amide proton of the alanine at the P1′ position in PA-pep formed an additional hydrogen bond with the carbonyl oxygen of Gly-115 located in the edge strand (Fig. 2*C*). As a consequence, the backbone of residues P1′ and P2′ was shifted by 1 Å (5 times the r.m.s.d. of the global backbone alignment) toward the N-terminal part of the edge strand in the PA-pep structure. This resulted in a sharper kink at the P1′ residue (Fig. 2*D*). The angle of the second kink of the PA-pep was very similar to those of AP-pep and PP-pep. This shift of the scissile peptide bond away from the metal ion–binding site in the PA-pep complex could explain the reduced k_{cat} of PPEP-1(WT) in the case of the substrate Abz-PA-Dnp.

To confirm that the substrate binding was not significantly influenced by the absence of the Zn^{2+} ion, cocrystallization experiments were repeated in the presence of 0.1 mM $ZnCl_2$. With PP-pep and PA-pep, only crystals of zinc-bound PPEP-1(E143A/Y178F) in complex with the unprimed fragment Ac-EVNP, *i.e.* the N-terminal cleavage product of the substrate peptides, were obtained (Tables S4 and S5). The reason for this was probably the remaining very low residual proteolytic activity of this PPEP-1 variant. However, a crystal structure of zinc-bound PPEP-1(E143A/Y178F) with uncleaved AP-pep was obtained (Table S5). The substrate peptide as well as the Zn^{2+} ion was well-resolved (Fig. 2*E*), and the binding mode was exactly the same as without the Zn^{2+} ion.

A comparison of the situation found in PPEP-1 with the related proteases thermolysin and anthrax LF, of which both do not prefer proline residues at the P1′ position, reveals some interesting aspects (Fig. 3). Notably, the hydrogen bond of the main-chain amide of the P1′ residue to the edge strand was also present in the structure of thermolysin in complexes with a substrate-mimicking inhibitor (PDB code 4N4E (14)) and in LF in complex with a substrate peptide (PDB code 1PWV (15)). In thermolysin and LF, there is also an interaction of the scissile-bond NH group with Asn-112 and Ser-655, respectively. The corresponding residue in PPEP-1 is Val-113, which is, as the following edge strand, shifted away by about 1 Å from the catalytic zinc ion compared with the equivalent residues in thermolysin and LF. This shift of the edge strand and the displacement of the valine residue in PPEP-1 were required to fit a proline residue at position P1′. Thermolysin and LF barely accepted substrates with a P1′ proline (15, 16), which can be explained by the resulting steric hindrance. In contrast, substrates with residues other than proline at the P1′ position are, upon binding to PPEP-1, translated by about 1 Å away from the catalytic zinc ion, leading to less efficient hydrolysis.

Lys-101 and Glu-184 of the (Lys-101, Glu-184, Glu-185, Asn-3) interaction interface to the substrate are essential for proteolytic activity*

In cocrystal structures of PPEP-1(E143/Y178F) with PP-pep, PA-pep, and AP-pep, the ϵ-amino group of Lys-101 in the S-loop was found to interact with the γ-carboxyl groups of Glu-184 and Glu-185 as well as with the oxygen atom of the asparagine β-amide group at position P2 (Asn-3*). Hereafter, we refer to this interface as the KEEN interface. The KEEN interface explains the strong preference of PPEP-1 for asparagine residues at substrate position P2 and was the only notable interaction of the S-loop with the lower rim of the substrate-binding cleft in the closed conformation (Fig. 4*A*). Furthermore, with the participation of Glu-185, this interface was directly linked to the coordination chemistry of the catalytic Zn^{2+} ion. To clarify these interactions, structural and kinetic investigations were carried out using mutants where Lys-101 was replaced by alanine, glutamate, or arginine.

A

Substrate	K_M [μM]	V_{max} [nM/s]	k_{cat} [s^{-1}]	k_{cat}/K_M [M^{-1} s^{-1}]
PP	137 ± 12.0	589.1 ± 40.7	4.3 ± 0.3	31386
AP	43.6 ± 12.0	170.9 ± 11.7	1.26 ± 0.09	28899
PA	82.5 ± 10.8	117.7 ± 5	0.87 ± 0.04	10545

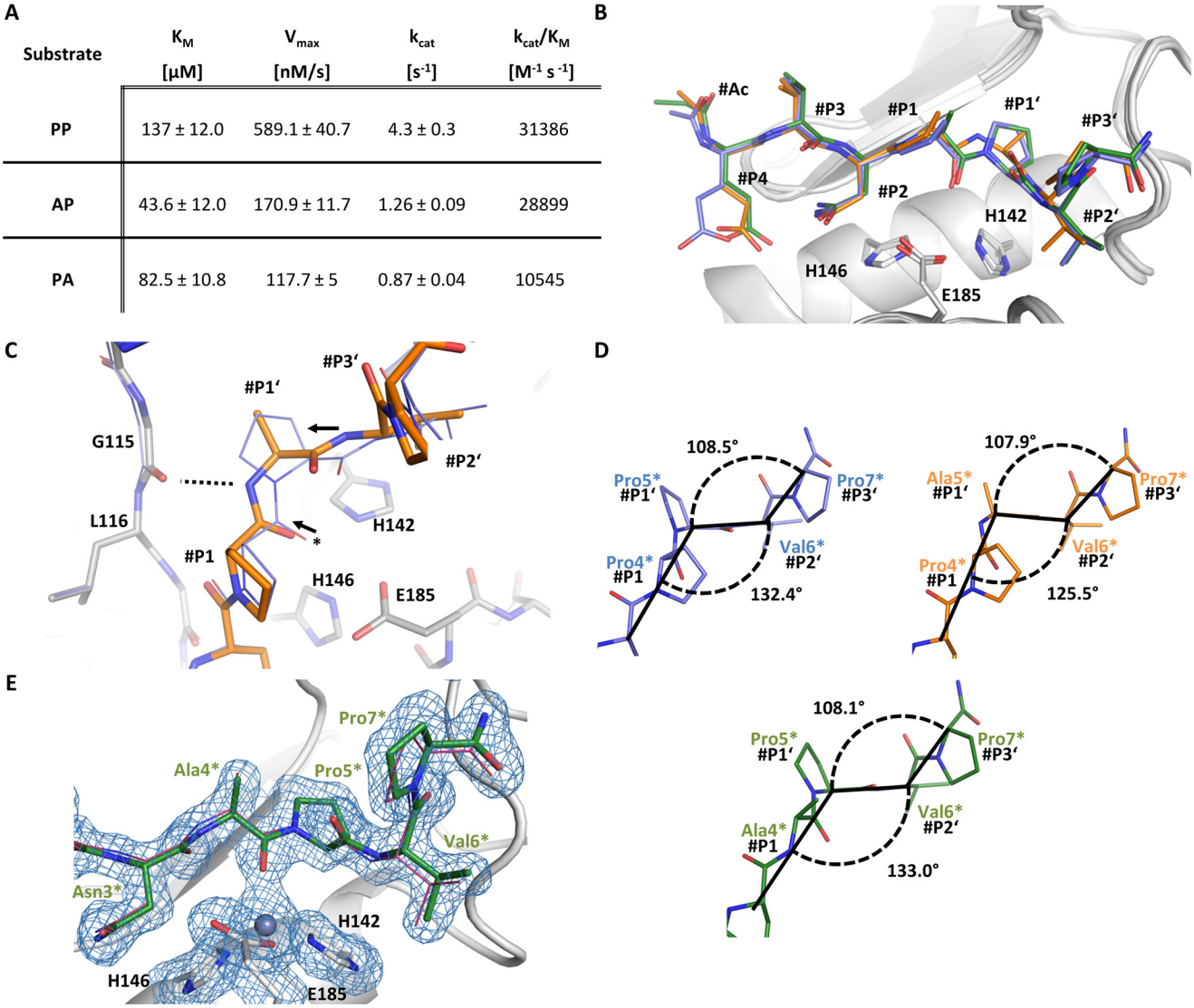

Figure 2. PPEP-1 prefers proline at P1 and P1′ positions. *A*, Michaelis–Menten parameters of PPEP-1(WT) for the substrates Abz-PP-Dnp, Abz-AP-Dnp, and Abz-PA-Dnp. *B*, superimposed structures of apo-PPEP-1(E143A/Y178F), PP-pep (*blue*), AP-pep (*green*), and PA-pep (*orange*) are shown. His-142, His-146, and Glu-185 in the active site of PPEP-1 are shown as *sticks*. Residues of the substrate peptides are marked with a *hash mark* (#) and named according to the Schechter and Berger (9) nomenclature (P4–P1 and P1′–P3′). For the sake of visibility, the S-loop is not shown. *C*, detail of the complex structure with PA-pep (*orange*). The nitrogen of the scissile bond forms a hydrogen bond (*dashed line*) to the carbonyl group of the peptide bond between Gly-115 and Leu-116 of PPEP-1. The residues at positions P1′ and P2′ of PA-pep are shifted toward the edge strand (Gly-115; *arrows*) compared with PP-pep. *D*, analysis of the backbone angles at residues P1′ and P2′. PP-pep, AP-pep, and PA-pep are colored in *blue*, *green*, and *orange*, respectively. Axes were fitted to the Cα atoms to calculate the kink angles using Chimera (39). *E*, $2F_o - F_c$ map of the complex structure of holo-PPEP-1(E143A/Y178F) with AP-pep. The contour level was set to 1 r.m.s.d. (0.408 e/Å^3). For comparison, AP-pep bound to apo-PPEP-1(E143A/Y178F) was superimposed and is shown as *thin pink lines*).

Crystal structures of the K101A and K101R mutants were determined at a resolution of 2.02 and 1.80 Å, respectively (Table S6). There were no major changes compared with the WT (PDB code 5A0P). The arginine residue in one protomer of the K101R mutant interacts with Glu-184 as expected. In the other protomer, it is displaced by a crystal contact. As in most other substrate peptide-free and zinc-bound structures, a Tris molecule from the buffer was coordinated to the catalytic zinc ion.

The specific activities of the K101A and K101E mutants against all three substrates, Abz-PP-Dnp, Abz-PA-Dnp, and Abz-AP-Dnp, were dramatically reduced (Fig. 4*B*), whereas the K101R mutant had a similar activity to the WT (Fig. 4*B*). Accordingly, the exchange of Glu-184 led to a strong reduction in activity. PPEP-1(E184K) showed only a residual activity against all three Abz/Dnp peptides (Fig. 4*B*), whereas the mutation E184A caused a decline in activity for Abz-PP-Dnp and Abz-AP-Dnp by 85 and 91%, respectively. Only a very small residual activity of 1.2% could be detected for Abz-PA-Dnp. The double mutation K101E/E184K could not restore the activity of the respective single mutants, probably because only two of the four interaction partners were swapped and/or the positive charge of the protonated lysine side chain was moved further away from the catalytic zinc ion. Crystal structures of the E184A, E184K, and E184K/K101E mutants had no major changes compared with the WT. However, both independent protomers of E184K and E184K/K101E are in the closed conformation.

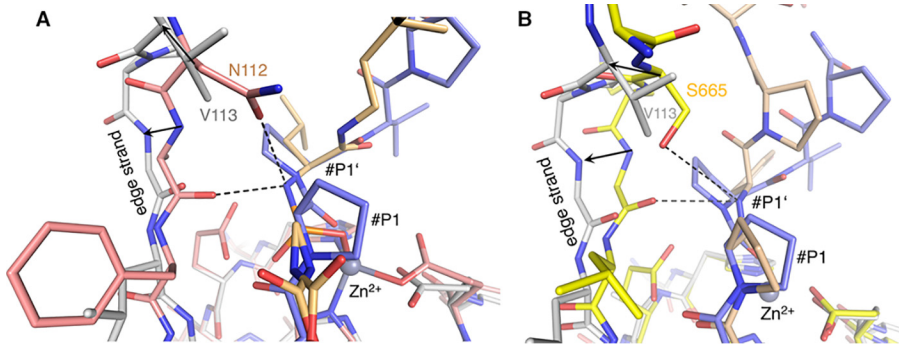

Figure 3. Structural basis for the proline specificity of PPEP-1 at position P1′ compared with thermolysin and lethal factor. *A* and *B*, superimposition of PPEP-1(E143A/Y178F) (*gray*) in complex with PP-pep (*blue*) with holo-thermolysin (*salmon*) with the substrate-mimicking inhibitor UBTLN85 (*wheat*) (*A*) and apo-anthrax LF (*yellow*) with substrate peptide (*wheat*) (*B*). Positions of P1 and P1′ residues are labeled in *black* and with a *hash mark*. Interactions between the scissile-bond NH group and protein components are shown as *black dotted lines*. Proline residues in P1′ position in thermolysin and LF are likely to be prohibited as this would introduce steric clashes with the carbonyl group of the edge strand interacting with the scissile-bond nitrogen as well as with Asn-112/Ser-665. *Black arrows* indicate that, in PPEP-1, residue Val-113 and the edge strand are shifted from the catalytic Zn^{2+}, thus creating space for substrates with a proline residue at position P1′ (PDB codes 5A0X, 4N4E, and 1PWV).

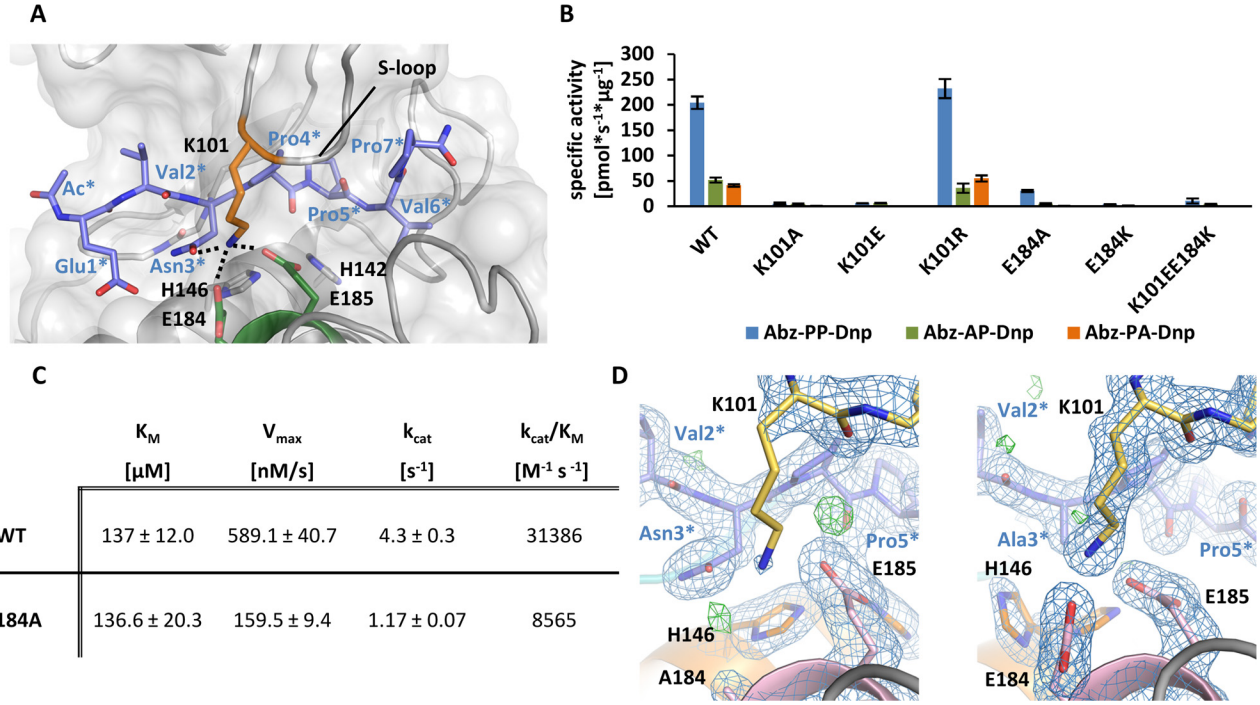

	K_M [µM]	V_{max} [nM/s]	k_{cat} [s^{-1}]	k_{cat}/K_M [M^{-1} s^{-1}]
WT	137 ± 12.0	589.1 ± 40.7	4.3 ± 0.3	31386
E184A	136.6 ± 20.3	159.5 ± 9.4	1.17 ± 0.07	8565

Figure 4. The KEEN interaction interface. *A*, crystal structure of PPEP-1(E143A/Y178F) in complex with PP-pep with detail of the KEEN interaction interface. The substrate peptide (PP-pep) is colored and labeled in *blue*. PPEP-1 components of the KEEN interface (Lys-101, *orange*; Glu-184 and Glu-185, *green*) and metal ion–coordinating histidine residues (His-142 and His-146; *gray*) are shown as *sticks*. PPEP-1 components are labeled *black*. Hydrogen bonds are indicated as *dotted lines* (PDB code 5A0X). *B*, specific activity of WT PPEP-1 and KEEN interaction interface mutants in the presence of Abz-PP-Dnp, Abz-AP-Dnp, or Abz-PA-Dnp. The measurements were carried out in triplicate. *Error bars* are the S.D. with average values above the *bars*. *C*, Michaelis–Menten parameters of PPEP-1(E184A) for substrate Abz-PP-Dnp. The same PPEP-1(WT) data are shown as in Fig. 1. *D*, the KEEN interaction interface is disrupted by the E184A mutation but not by the absence of Asn-3* in the substrate peptide. The KEEN interaction interface of both cocrystal structures with PP-pep (*left*) or APP-pep (*right*) is shown. The substrate peptide is colored in *blue*, the S-loop is in *yellow*, the active-site helix is in *orange*, and the gluzincin characteristic helix is in *pink*. The electron density ($2mF_o - DF_c$) around the substrate peptide, catalytic Zn^{2+} ions, and the side chains of Lys-101, His-142, His-146, Ala-184, and Glu-185 is shown at a contour level of 1 r.m.s.d. (0.31 e/Å^3). The difference electron density ($mF_o - DF_c$) is shown as *green mesh* with a contour level of +3 r.m.s.d. (0.31 e/Å^3).

To analyze the role of the KEEN interaction interface with regard to the proteolytic mechanism, the kinetic parameters of PPEP-1(E184A) in the presence of the Abz-PP-Dnp substrate were determined. Compared with the WT, the E184A mutant had a 3.6-fold reduced k_{cat} value, whereas K_m remained unchanged (Fig. 4*C*), thus suggesting that the KEEN interface is important for efficient catalysis.

To investigate the structural effects of the E184A mutation, the triple mutant PPEP-1(E143A/Y178F/E184A) was cocrystallized with PP-pep and AP-pep. Crystals of PPEP-1(E143A/Y178F/E184A) with PP-pep diffracted to a resolution of 1.9 Å (Table S7). The substitution was clearly visible in the electron density map, whereas the side chain of Lys-101 was only poorly resolved in both protomers, thus indicating that its interactions with Glu-185 and the substrate peptide's Asn-3* were strongly reduced (Fig. 4*D*). Interestingly, despite disruption of the KEEN interface, the S-loops of both PPEP-1 protomers were nevertheless found in the closed conformation. This indicates that other interactions between substrate peptide and the S-loop suffice for loop closure.

Table 3

Sequences of peptides with noncanonical cleavage sites used for cocrystallization

N, acetylated N terminus; P4–P3′, residue position in the substrate-binding cleft of PPEP-1 according to Schechter and Berger (9); C, C terminus; $CONH_2$, amidated C terminus; AA, amino acid.

	Position								
Name	N	P4	P3	P2	P1	P1′	P2′	P3′	C
IgA1-pep	Ac	His	Leu	Leu	Pro	Pro	Pro	Ser	$CONH_2$
Hsp90-pep	Ac	Glu	Pro	Asn	Ala	Ala	Val	Pro	$CONH_2$
Fib-pep	Ac	Ser	Leu	Arg	Pro	Ala	Pro	Pro	$CONH_2$
AA position		1	2	3	4	5	6	7	

PPEP-1(E143A/Y178F/E184A) in complex with AP-pep yielded a different orthorhombic crystal form (Table S4). All four protomers in the asymmetric unit were similar to the structure of this triple mutant in complex with the PP-pep peptide. The KEEN interaction interface was again disrupted with a disordered side chain of Lys-101 in all four protomers, thus confirming that the E184A mutation strongly reduced the interaction of Lys-101 with Glu-185 and Asn-3*.

To assess the influence of the asparagine residue at position P2 in PPEP-1 substrates on the formation of the KEEN interaction interface, PPEP-1(E143A/Y178F) was cocrystallized with substrate peptide APP-pep in which the canonical asparagine residue Asn-3* at the P2 position was replaced by an alanine (Tables 2 and S8). APP-pep was bound to PPEP-1 in a conformation identical to that observed for PP-pep. This suggested that the asparagine side chain was not required for proper positioning of the substrate. Furthermore, the electron density of the side chain of Lys-101 was fully defined in both PPEP-1 protomers present in the asymmetric unit (Fig. 4*D*). Lys-101 was also bound here to the γ-carboxylate groups of Glu-184 and Glu-185, indicating that an asparagine residue at the substrate P2 was not strictly required for this interaction, although it probably contributed to its stability.

Recognition of other substrates with noncanonical sequences

PPEP-1 has been reported to cleave *in vitro* IgA1/IgA2, Hsp90β, and fibrinogen at noncanonical recognition sequences (1, 2). To analyze the molecular details of the recognition of such substrates, PPEP-1(E143A/Y178F) crystallization trials with peptides containing the corresponding sequences of IgA1, Hsp90β, and fibrinogen were set up (Table 3). Crystals were obtained only with the substrate peptide of fibrinogen (Fib-pep; SLRP ↓ APP) (Table S5). It contained three PPEP-1 molecules in the asymmetric unit. All three protomers showed a high similarity to the structure of PPEP-1(E143A/Y178F) with PP-Pep (PDB code 5A0X) with an r.m.s.d. of about 0.9 Å for all residues.

The Fib-pep was well-defined in the electron density map of all three protomers. Here as well, a metal-free protein–peptide complex structure was obtained. Fib-pep also bound to PPEP-1 in a double-kinked manner (Fig. 5). Residues Leu-2*, Pro-4*, Ala-5*, Pro-6*, and Pro-7* of Fib-pep bound very similarly to the respective subsites as their counterparts in PP-pep. As observed in the complex structure of PA-pep, the amide NH group of the scissile bond again formed a hydrogen bond with the carbonyl group of Gly-115 located in the edge strand. As in all other substrate complexes, the main-chain carbonyl group of the P1′ residue (Ala-5*) was hydrogen-bonded to the NH group of the indole ring of Trp-103. Pro-6* (at P2′) was bound by several van der Waals interactions to Ala-136, His-142, and Asn-175. Furthermore, it formed a parallel-displaced aromatic–aliphatic stacking to Phe-178, and its carbonyl group accepted a hydrogen bond from the main-chain amide of Asp-135. Pro-7* (at P3′) was bound by a T-shaped displaced aliphatic–aromatic stacking to Phe-178 and by a parallel aliphatic–aromatic stacking to Trp-103.

Notably, the arginine residue (Arg-3*) of Fib-pep at position P2 bound differently in the three protomers present in the asymmetric unit. In two protomers, its side chain protruded into a negatively charged pocket formed by Asp-149 and Asp-155 (Fig. 5*A*), displacing the second coordination-sphere water molecule interacting with His-146 of the ^{142}HE*XX*H^{146} motif. In the third protomer, its guanidinium moiety interacted with Glu-184 and Glu-185 (Fig. 5*B*). As a result, Lys-101 was displaced.

Hydrogen bonding of the substrate by Trp-103 is crucial for effective peptide bond hydrolysis

Crystal structures of peptide-bound PPEP-1 provided strong indications that the S-loop closes upon substrate peptide binding. Apart from Lys-101 as a part of the KEEN interaction interface, Pro-100 and Trp-103 were also found to be present in the S-loop. Both residues belong to a large aromatic–aliphatic network containing Tyr-94, Leu-95, Pro-100, Trp-103, and Trp-110 located in the upper rim of the substrate-binding cleft (Fig. 5*A*) (10). In the substrate-bound state, Trp-103 interacted in a parallel aliphatic–aromatic interaction with the proline residue of the substrate at position P3′ (Pro-7*), which agrees with the previous finding that tryptophan was the most preferred amino acid to form aromatic–aliphatic stackings with prolines (17). Moreover, its indole ring ϵ-NH group forms an H-bond to the carbonyl oxygen of the P1′ proline (Pro-5*). We probed the importance of Trp-103 for proteolytic activity of PPEP-1 by generating mutants W103A, W103F, W103Y, and W103H. These proteins showed no difference in their thermal stabilities compared with WT PPEP-1 (Table S10), but all of them were almost inactive against Abz-PP-Dnp, Abz-PA-Dnp, and Abz-AP-Dnp (Fig. 6*B*).

A crystal structure of the W103F mutant was similar to other substrate-free PPEP-1 structures but again with two "closed" protomers in the asymmetric unit. Again, there is a Tris molecule bound to the zinc ion (Table S8).

For further analysis, the triple mutants E143A/Y178F/W103F and E143A/Y178F/W103H were cocrystallized with PP-pep. The structure revealed no major changes in either protease or substrate conformation. The phenylalanine side chain of the W103F mutant interacted in a manner similar to

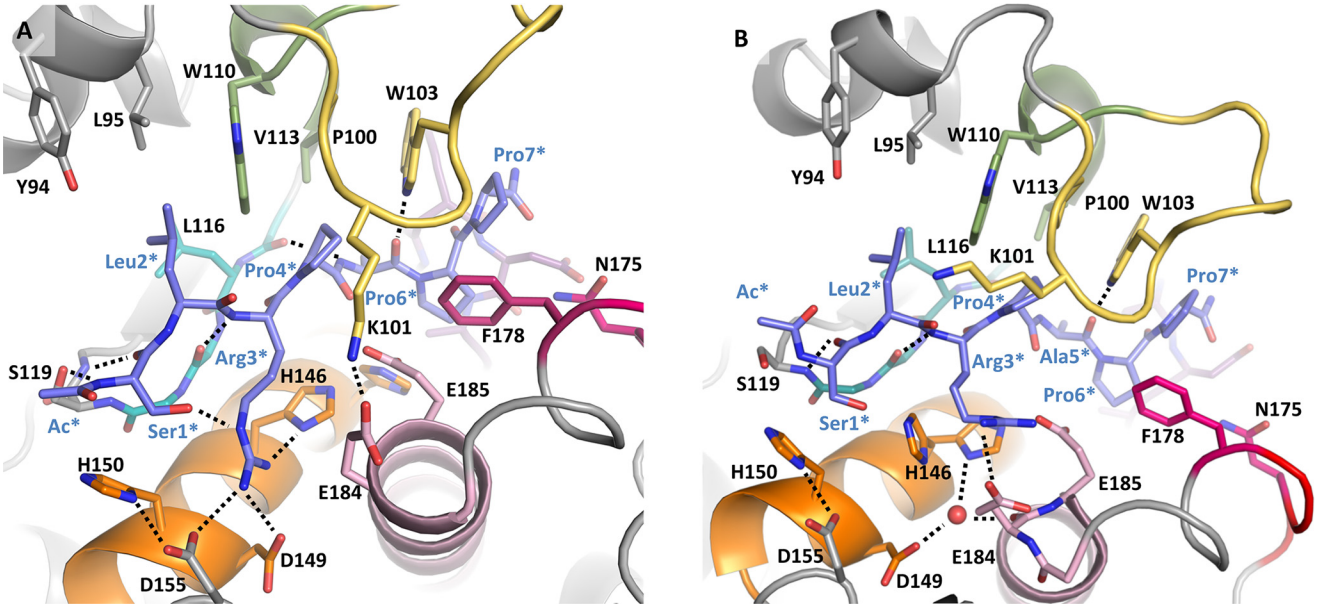

Figure 5. Alternating binding modes of Arg-3* at the P2 position in the Fib-pep complex. The S-loop is shown in *yellow*, the bulge-edge segment is in *green*, the edge strand is in *cyan*, the diverting loop is in *purple*, the active-site helix is in *orange*, the gluzincin helix is in *pink*, and the S1′-wall–forming segment is in *red*. Metal ion–coordinating residues and amino acids interacting with the substrate peptide (*blue*) are shown as *sticks* and are labeled in *black*. Substrate peptide residues are labeled in *blue*. Hydrogen bonds are indicated as *dotted lines*. *A*, the situation in two crystallographic independent protomers. *B*, in the third protomer Arg-3* undergoes a different set of interactions.

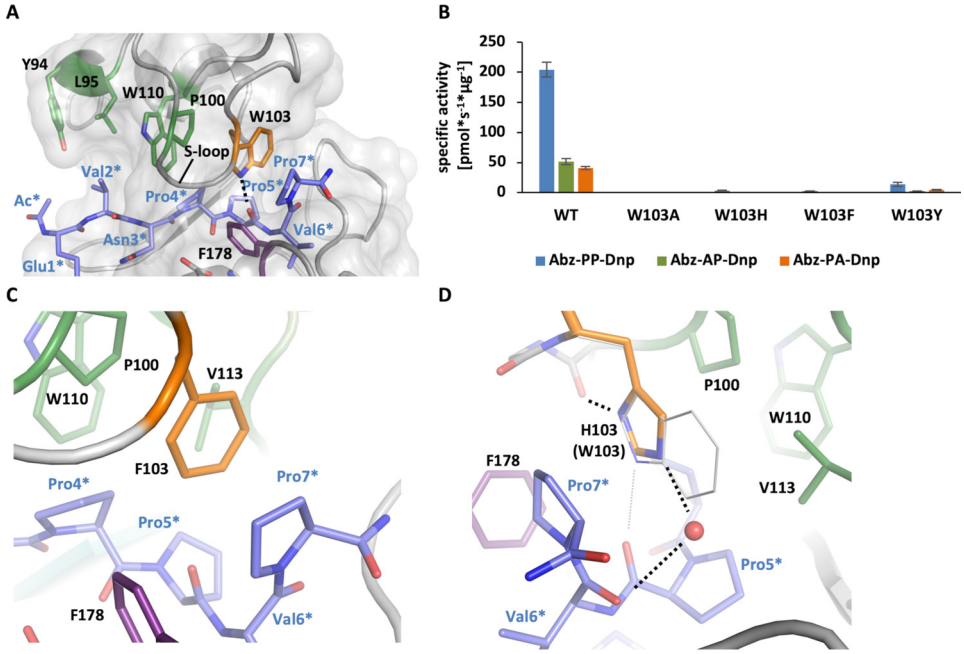

Figure 6. Trp-103 is crucial for PPEP-1 activity. *A*, Trp-103 is part of the aliphatic–aromatic network together with Tyr-94, Leu-95, Pro-100, and Trp-110. The aliphatic–aromatic network is colored in *green*, Trp-103 is in *orange*, the substrate peptide is in *blue*, and Phe-178 is in *violet*. The hydrogen bond between Trp-103 and the carbonyl oxygen of the P1′ residue is shown as a *dashed line*. Residues of the substrate peptides are labeled in *blue* and indicated by an *asterisk*. PPEP-1 residues are labeled *black* (PDB code 5A0X). *B*, specific activity of WT and Trp-103 mutants with substrates Abz-PP-Dnp, Abz-AP-Dnp, and Abz-PA-Dnp. The measurements were carried out in triplicate. *Error bars* are the S.D. with average values above the *bars*. *C*, focus on the primed part of the substrate-binding cleft of PPEP-1 in the complex structure of PPEP-1(W103F/E143A/Y178F) with PP-pep. Structural elements of PPEP-1(W103F/E143A/Y178F) and PP-pep are colored as follows. The substrate peptide is *blue*, residues of the aliphatic–aromatic network are in *green* color, and Phe-178 is in *pink*. Substrate residues are labeled *blue*, and protein residues are labeled *black*. *D*, a similar close-up view of the complex structure of PPEP-1(W103H/E143A/Y178F) with PP-pep. Color coding is as in *C*. Hydrogen bonds are shown as *black dashed lines*. The complex structure of PPEP-1(E143A/Y178F) with PP-pep is superimposed. Trp-103 of PPEP-1(E143A/Y178F) is indicated as *thin lines*. The hydrogen bond between Trp-103 and the peptide bond between P1′ and P2′ are indicated as *thin dashed lines*.

that of the WT with Pro-100, Val-113, and the proline at position P3′ of the substrate peptide (Fig. 6*C*). The strongly diminished activity of the W103F mutant demonstrated the importance of the hydrogen bond between residue 103 and the carbonyl oxygen of the P1′ substrate residue for proteolytic activity (Fig. 6*B*).

Based on simple modeling, we hypothesized that the W103H mutant would be active because an imidazole side chain at posi-

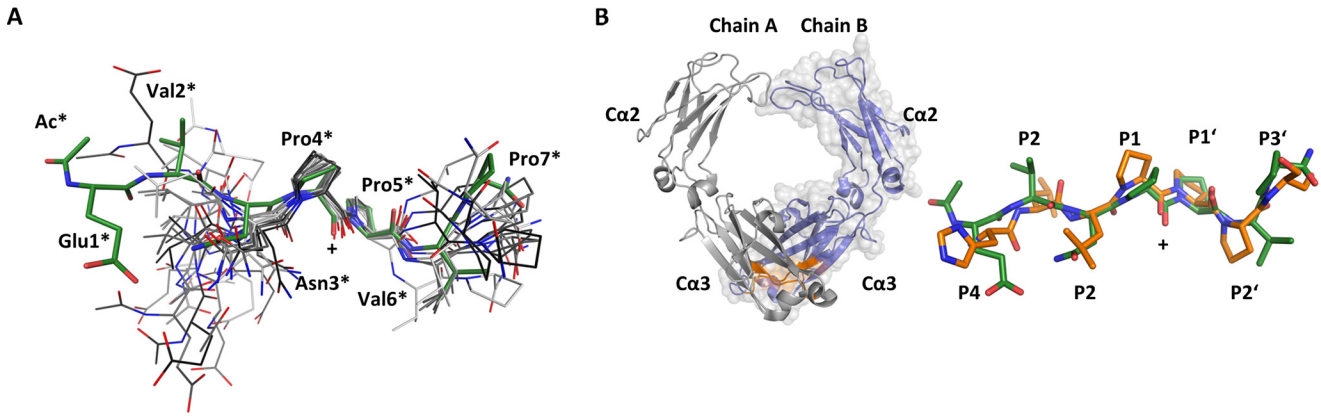

Figure 7. Conformation of PPEP-1 substrate peptides in solution and in other substrate proteins. *A*, the 10 lowest-energy models determined by NMR in solution of PP-pep (*gray*) were superimposed with the crystal structure (*green*; PDB code 5A0X). For clarity, hydrogen atoms are not shown. Residues are labeled, and the scissile bond is marked with a *black cross*. *B*, the conformation of the PPEP-1–recognition sequence in IgA1 resembles the conformation of PPEP-1–bound PP-pep. *Left*, cartoon representation of the Fc region of IgA1 (PDB code 2QEJ (18)). Chains are colored either *blue* or *gray*. The PPEP-1–recognition site is colored *orange*. *Right*, superimposition of the PPEP-1–recognition site in IgA1 (*orange*) and PPEP-1–bound PP-pep (*green*; PDB code 5A0X).

tion 103 could also hydrogen-bond to the P1′ proline. However, PPEP-1(W103H) was virtually inactive (Fig. 6*B*). In the crystal structure (Table S9), the side-chain imidazole group was flipped with respect to the indole group of the WT, and the δ-nitrogen of His-103 was hydrogen-bonded to the main-chain carbonyl oxygen of Lys-101 and not to the carbonyl oxygen of the P1′ residue (Fig. 6*D*). Moreover, His-103 bound to the carbonyl group of the substrate of the P2′ residue via a water bridge in one protomer. Thus, the hydrogen bond between the side chain of His-103 and the P1′ residue was not present, similar to the likewise inactive W103F mutant.

PPEP-1 substrates possess a preorganized conformation complementary to the shape of the substrate-binding cleft

We also analyzed the solution structure of PP-pep (Figs. 7*A*, S5–S8, and Table S11). Superimposition of the solution structure of PP-pep with the PPEP-1–bound peptide revealed that the conformations of the P2–P2′ residues were similar. The first kink (at P1′) was already present in solution. The second kink at P2′ was also preformed, albeit to a lesser extent. This showed that in solution the PP-pep substrate already adopted a conformation at residues Asn-3*–Pro-7* that was similar to the PPEP-1–bound conformation in the crystal structure. It is therefore likely that the PPEP-1 cleavage sites in CD2831 and CD3246 have a similar conformation. Supporting this suggestion, a noncanonical PPEP-1 cleavage site in IgA (at residues 231 to 237) (PDB code 2QEJ (18)) exhibited virtually the same conformation as PP-pep (Fig. 7*B*). There were also two kinks in the primed region, which were most likely stabilized by the steric rigidity of the proline residues.

Taking this into account, we propose that the shape of the substrate-binding groove follows the local structure of the cleavage site. As the accessible values of the backbone torsion angle Φ of proline residues is very restricted compared with all other amino acids, only a relatively small amount of substrate conformational entropy is lost upon binding to PPEP-1. This might be a key element for the substrate recognition by PPEP-1.

Discussion

In this and a previous study (2), the preference of PPEP-1 for Pro-Pro peptide bonds was shown. Replacement of the P1 or P1′ proline by alanine diminished the activity, but the reduction was more pronounced for the P1′ position.

This study provides new structural and mechanistic insights into the specificity and substrate recognition of PPEP-1. The most important findings are that PPEP-1 discriminated between alanine and proline residues at position P1′ based on the hydrogen-bonding potential of the amide group of this residue, where the donation of an H-bond by the substrate to the edge strand leads to a small shift from the catalytic center and therefore to a reduced k_{cat} value. Furthermore, residues other than proline suffer from a greater entropy loss upon binding to the enzyme. For efficient catalysis, the S-loop has to be properly closed. It has previously been shown that deletion of the S-loop together with the bulge-edge segment (Δ92–114) resulted in a complete inactivation of PPEP-1 (11). In the work presented here, Trp-103 of the aliphatic–aromatic network and the KEEN interaction interface, with both of them being responsible for anchoring the S-loop to the substrate and the lower rim of the active-site cleft, were identified as essential for proteolytic activity. Noteworthy is the observation that Glu-184 is not strictly conserved. For example, in PPEP-2 from *Paenibacillus alvei* it is replaced by a threonine. PPEP-2 does not favor an asparagine in P2 position but a leucine (19), and Lys-101 is replaced by an arginine. Whether this leads to different interactions is unclear due to the lack of a substrate complex structure of PPEP-2.

We finally propose an induced-fit mechanism (Fig. 8) in which prestructured substrates are also recognized by the aliphatic–aromatic network. The substrate peptide is then bound in the doubly kinked substrate-binding groove, and, as a result, the KEEN interaction interface is formed, thus also changing the second coordination sphere of the catalytic zinc ion. The placement of a positive charge in the second coordination sphere of the catalytic zinc ion would increase the acidity of the zinc-bound water molecule (20) and therefore enhance

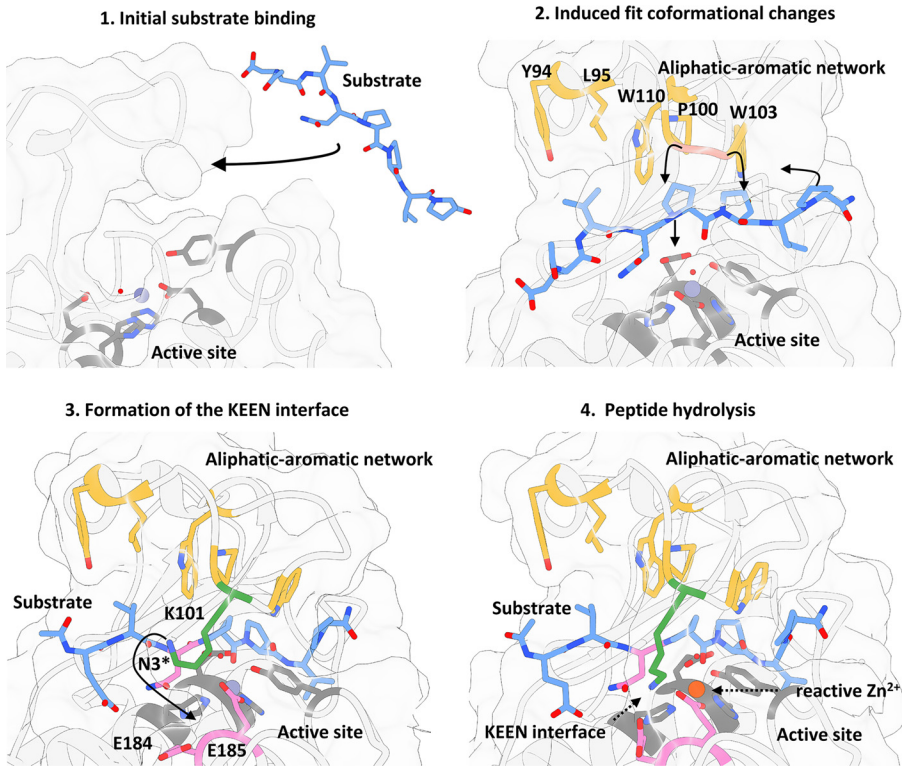

Figure 8. Proposed model of PPEP-1 substrate recognition. During initial binding to PPEP-1 (*1*), the prestructured substrate (*blue*) starts to interact with the aliphatic–aromatic network (*yellow*). These interactions trigger an induced-fit mechanism in which the S-loop closes and the substrate is correctly positioned in the substrate-binding cleft (*2*). Upon S-loop closure, the KEEN interaction interface (*pink*) forms (*3*), not only stabilizing the S-loop in its closed conformation but also increasing the reactivity of the catalytic zinc ion by changing its secondary coordination sphere via Lys-101 (*green*) and enabling an efficient peptide hydrolysis (*4*).

catalysis. It is known from other metalloenzymes (21) and inorganic or organic metallocomplexes that the second coordination sphere influences the reactivity of a catalytic metal ion (22–25). This most likely also holds for metallopeptidases.

Experimental procedures

Peptides

All peptides were purchased from GenScript with a purity of at least 90%.

Site-directed mutagenesis

Mutations were introduced by the QuikChange™ site-directed mutagenesis method developed by Stratagene (La Jolla, CA). Mutagenizing primers (Table S12) were designed according to Zheng (26).

Production of PPEP-1 proteins

WT PPEP-1 and PPEP-1 mutants were recombinantly produced in *E. coli* BL21 Star (DE3) cells using pET28a-based expression vectors as described (27). The purification process was evaluated by SDS-PAGE analysis of samples taken during immobilized metal-affinity chromatography and size-exclusion chromatography (Figs. S9 and S10)

Fluorescence-based thermal shift assay

Fluorescence-based thermal shift assays (28) were performed in a CFX 96 Real-Time PCR Detection System (Bio-Rad). T_m was determined by using the internal algorithms of the data analysis software (Bio-Rad CFX Manager™, version 3.1.1517.0823).

Preparation of Abz/Dnp substrate peptide stock solutions

Lyophilizates were solubilized in 100% DMSO to a concentration of 20–30 mM and subsequently diluted 1:19 with 20 mM Hepes, pH 7.5, 200 mM NaCl (HBS). Concentrations of the peptides were determined spectrophotometrically at 365 nm using the molar extinction coefficient (ϵ_{365} = 17,300 M^{-1} cm^{-1}) of the Dnp group (29). Stock solutions were adjusted to a concentration of 1 mM substrate peptide using HBS supplemented with 5% DMSO.

Determination of the specific activity of PPEP-1 variants

Assays for determining relative activities were performed in triplicate using a BioTek Synergy H4 plate reader and repeated at least once. Fluorescence was measured at the excitation and emission wavelengths of 320 ± 20 and 420 ± 20 nm, respectively. Activity assays were performed in a total volume of 100 μl composed of 5 μl of protein (diluted in HBS), 90 μl of HBS, and 5 μl of 1 mM Abz/Dnp substrate in HBS with 5% DMSO. Reactions were started by adding 5 μl of substrate solution. Initial slopes in regions where fluorescence increase was linear were used to determine the activity of each PPEP-1 variant.

The determination of Michaelis–Menten kinetic parameters was performed in rectangular Suprasil quartz glass cuvettes (105.252-QS, Hellma Analytics) using a Fluoromax-4 fluorimeter (HORIBA Scientific). Initial velocities were recorded at substrate concentrations of 12.5, 25, 50, 75, 100, 150, 200, 250, 300, 350, and 400 μM. Each reaction had a total volume of 35 μl composed of 5 μl of enzyme solution (0.02 mg/ml PPEP-1 in 20 mM Hepes, pH 7.5, 200 mM NaCl, 0.05% Triton X-100) and 30 μl of substrate solution

containing the substrate and 20 mM Hepes, pH 7.5, 200 mM NaCl, 5% DMSO. The excitation beam had a wavelength of 320 ± 2.4 nm, and emission was detected at 420 ± 2 nm with an integration time of 0.5 s and a total recording time of 600 s.

Inner filter effects were corrected with the following formula (12).

$$F_{corr} = F_{obs} \times \frac{2.3dA_{ex}}{1 - 10^{-dA_{ex}}} \times 10^{gA_{em}} \times \frac{2.3sA_{em}}{1 - 10^{-sA_{em}}} \quad \text{(Eq. 1)}$$

Here, F_{corr} and F_{obs} are the corrected and uncorrected fluorescence intensities, and A_{ex} and A_{em} are the absorbance values at the excitation and emission wavelengths. s is the width of the incident excitation beam, g is the distance from the edge of the excitation light beam to the edge of the sample chamber of the cuvette, and d is the width of the cuvette seen by the detector.

Inner-filter correction factors were determined using 400 μM Abz-PP-Dnp, Abz-AP-Dnp, or Abz-PA-Dnp digested with high amounts of PPEP-1 (1 mg/ml) for 30 min at 20 °C. Fluorescence was measured with the same instrumental setup as for the kinetic measurements to obtain F_{obs}, and a UV-visible spectrum was recorded to obtain A_{ex} and A_{em}. Afterward, solutions in the cuvettes were successively diluted, and fluorescence and UV-visible spectra were recorded. The data obtained were used to calculate the inner-filter correction factors and to generate a calibration curve to convert fluorescence increase velocities (cps/s) into molar activity (μmol/s) (Fig. S1). To determine k_{cat} and K_m, initial velocities, v_0, were plotted against the initial substrate concentrations, [S], and a curve was fitted to the data using the Michaelis–Menten equation (Fig. S11) using GraphPad prism software (version 6.02, GraphPad Software, Inc.).

Crystallographic methods

All crystals were obtained in $(NH_4)_2HPO_4$ grid screens at 20 °C as described previously (27). For cocrystallization experiments of PPEP-1 variants with peptides (PPEP-1–peptide complexes), a 10-fold molar excess of peptide was used. Crystals were cryoprotected by 30% (w/v) sucrose and flash-cooled in liquid nitrogen.

Diffraction data were collected at beamlines X06DA and X06SA of the Swiss Light Source (Paul Scherrer Institute, Villigen, Switzerland); at beamline P13 of PETRA/European Molecular Biology Laboratory (EMBL) Hamburg (German Synchrotron Research Center (Deutsches Elektronen-Synchrotron (DESY)) campus, Germany); and at beamlines ID23-1, ID29, ID30A-1, and ID30A-3 of the European Synchrotron Radiation Facility (ESRF; Grenoble, France). All data were processed using XDS and XSCALE (30).

Structure determination and refinement

Structures were determined using the WT PPEP-1 structure (PDB code 5A0P) as an initial model and either employing rigid-body refinement using phenix.refine (31) or molecular replacement as implemented in Phaser of the Phenix package (32). Structures were rebuilt manually using Coot (33) between iterative cycles of refinement using phenix.refine. Data collection and refinement statistics are summarized in Tables S3–S9.

NMR spectroscopy

All compounds used for the preparation of the buffer (*i.e.* sodium phosphate mono- and dibasic), d_6-2,2-dimethyl-2-silapentane-5-sulfonic acid (DSS), and deuterated water were purchased from Sigma-Aldrich. The samples were prepared by dissolving the peptide powder at a concentration ~1–3 mM in PBS buffer (200 μl; pH 7.0; H_2O/D_2O, 9:1; 3-mm NMR tubes). NMR spectra were recorded on a Bruker Avance II+ spectrometer (^{1}H frequency of 600 MHz) equipped with a triple-resonance high-resolution probe (TBI). All NMR data were acquired and processed using Topspin software (Bruker). The transmitter frequency was set on the HDO/H_2O signal, and the d_6-DSS resonance was used as chemical shift reference (^{1}H $\delta_{DSS} = 0$ ppm).

For assignment, 2D homo- and heteronuclear spectra (*i.e.* 2D ^{1}H,^{1}H total correlated spectroscopy (TOCSY), ^{1}H,^{1}H rotating-frame Overhauser spectroscopy (ROESY), ^{1}H,^{13}C heteronuclear single-quantum coherence (HSQC), and ^{1}H,^{13}C heteronuclear multiple-bond correlation (HMBC)) were recorded using standard Bruker pulse sequences, including excitation sculpting with gradients for solvent suppression (34).

The temperature dependence of the amide protons of peptide PP-pep was calculated from the shift of the amide protons within the range of 278–335 K. The complete assignment of the backbone and side-chain ^{1}H resonances was performed using standard sequential assignment procedures according to the methodology developed by Wüthrich (35) and analyzed using CARA software (36). Three-dimensional structures were determined by the standard protocol of the CYANA program (version 2.1) (37).

Author contributions—C. P., D. D., and U. B. formal analysis; C. P., L. J., and D. D. validation; C. P., L. J., F. W., and M. S. investigation; C. P. and L. J. visualization; C. P. methodology; C. P. and U. B. writing-original draft; M. S., D. D., and U. B. supervision; D. D. and U. B. resources; D. D. data curation; U. B. conceptualization; U. B. funding acquisition.

Acknowledgments—We thank the staff of beamlines X06SA and X06DA at the Swiss Light Source, Paul Scherrer Institute, Villigen, Switzerland, and ID23-1, ID29, ID30A-1 and ID30A3 at the European Synchrotron Radiation Facility (ESRF), Grenoble, France as well as P13 at the Deutsches Elektronen-Synchrotron (DESY), Hamburg, Germany for support during data collection. Crystals were grown in the Cologne Crystallization facility (C$_2$f). This work was supported by German Research Foundation Grant INST 216/ 682-1 FUGG for the Crystallization Facility, and the iNEXT initiative (European Union program Horizon 2020, pid 1859), and the European Community's Seventh Framework Program (FP7/2007–2013) under Grant Agreement 283570 (BioStruct-X) for the synchorotron access. The authors declare that they have no conflicts of interest with the contents of this article. D. D. is very grateful to the University of Cologne for supporting the JobSharing project.

References

1. Cafardi, V., Biagini, M., Martinelli, M., Leuzzi, R., Rubino, J. T., Cantini, F., Norais, N., Scarselli, M., Serruto, D., and Unnikrishnan, M. (2013) Identification of a novel zinc metalloprotease through a global analysis of *Clostridium difficile* extracellular proteins. *PLoS One* **8,** e81306 CrossRef Medline
2. Hensbergen, P. J., Klychnikov, O. I., Bakker, D., van Winden, V. J., Ras, N., Kemp, A. C., Cordfunke, R. A., Dragan, I., Deelder, A. M., Kuijper, E. J.,

Corver, J., Drijfhout, J. W., and van Leeuwen, H. C. (2014) A novel secreted metalloprotease (CD2830) from *Clostridium difficile* cleaves specific proline sequences in LPXTG cell surface proteins. *Mol. Cell. Proteomics* **13,** 1231–1244 CrossRef Medline

3. Bordeleau, E., and Burrus, V. (2015) Cyclic-di-GMP signaling in the Gram-positive pathogen *Clostridium difficile*. *Curr. Genet* **61,** 497–502 CrossRef Medline
4. Soutourina, O. A., Monot, M., Boudry, P., Saujet, L., Pichon, C., Sismeiro, O., Semenova, E., Severinov, K., Le Bouguenec, C., Coppée, J. Y., Dupuy, B., and Martin-Verstraete, I. (2013) Genome-wide identification of regulatory RNAs in the human pathogen *Clostridium difficile*. *PLoS Genet.* **9,** e1003493 CrossRef Medline
5. Peltier, J., Shaw, H. A., Couchman, E. C., Dawson, L. F., Yu, L., Choudhary, J. S., Kaever, V., Wren, B. W., and Fairweather, N. F. (2015) Cyclic diGMP regulates production of sortase substrates of *Clostridium difficile* and their surface exposure through ZmpI protease-mediated cleavage. *J. Biol. Chem.* **290,** 24453–24469 CrossRef Medline
6. Walden, M., Edwards, J. M., Dziewulska, A. M., Bergmann, R., Saalbach, G., Kan, S. Y., Miller, O. K., Weckener, M., Jackson, R. J., Shirran, S. L., Botting, C. H., Florence, G. J., Rohde, M., Banfield, M. J., and Schwarz-Linek, U. (2015) An internal thioester in a pathogen surface protein mediates covalent host binding. *Elife* **4,** e06638 CrossRef Medline
7. Corver, J., Cordo', V., van Leeuwen, H. C., Klychnikov, O. I., and Hensbergen, P. J. (2017) Covalent attachment and Pro-Pro endopeptidase (PPEP-1)-mediated release of *Clostridium difficile* cell surface proteins involved in adhesion. *Mol. Microbiol.* **105,** 663–673 CrossRef Medline
8. Hensbergen, P. J., Klychnikov, O. I., Bakker, D., Dragan, I., Kelly, M. L., Minton, N. P., Corver, J., Kuijper, E. J., Drijfhout, J. W., and van Leeuwen, H. C. (2015) *Clostridium difficile* secreted Pro-Pro endopeptidase PPEP-1 (ZMP1/CD2830) modulates adhesion through cleavage of the collagen binding protein CD2831. *FEBS Lett.* **589,** 3952–3958 CrossRef Medline
9. Schechter, I., and Berger, A. (1967) On the size of the active site in proteases. I. Papain. *Biochem. Biophys. Res. Commun.* **27,** 157–162 CrossRef Medline
10. Schacherl, M., Pichlo, C., Neundorf, I., and Baumann, U. (2015) Structural basis of proline-proline peptide bond specificity of the metalloprotease Zmp1 implicated in motility of *Clostridium difficile*. *Structure* **23,** 1632–1642 CrossRef Medline
11. Rubino, J. T., Martinelli, M., Cantini, F., Castagnetti, A., Leuzzi, R., Banci, L., and Scarselli, M. (2016) Structural characterization of zinc-bound Zmp1, a zinc-dependent metalloprotease secreted by *Clostridium difficile*. *J. Biol. Inorg. Chem.* **21,** 185–196 CrossRef Medline
12. Gauthier, T. D., Shane, E. C., Guerin, W. F., Seitz, W. R., and Grant, C. L. (1986) Fluorescence quenching method for determining equilibrium constants for polycyclic aromatic hydrocarbons binding to dissolved humic materials. *Environ. Sci. Technol.* **20,** 1162–1166 CrossRef
13. Lovell, S. C., Davis, I. W., Arendall, W. B., 3rd, de Bakker, P. I., Word, J. M., Prisant, M. G., Richardson, J. S., and Richardson, D. C. (2003) Structure validation by Cα geometry: ϕ,ψ and Cβ deviation. *Proteins* **50,** 437–450 CrossRef Medline
14. Krimmer, S. G., Betz, M., Heine, A., and Klebe, G. (2014) Methyl, ethyl, propyl, butyl: futile but not for water, as the correlation of structure and thermodynamic signature shows in a congeneric series of thermolysin inhibitors. *Chem. Med. Chem.* **9,** 833–846 CrossRef Medline
15. Turk, B. E., Wong, T. Y., Schwarzenbacher, R., Jarrell, E. T., Leppla, S. H., Collier, R. J., Liddington, R. C., and Cantley, L. C. (2004) The structural basis for substrate and inhibitor selectivity of the anthrax lethal factor. *Nat. Struct. Mol. Biol.* **11,** 60–66 CrossRef Medline
16. Vidmar, R., Vizovišek, M., Turk, D., Turk, B., and Fonović, M. (2017) Protease cleavage site fingerprinting by label-free in-gel degradomics reveals pH-dependent specificity switch of legumain. *EMBO J.* **36,** 2455–2465 CrossRef Medline
17. Zondlo, N. J. (2013) Aromatic-proline interactions: electronically tunable CH/π interactions. *Acc. Chem. Res.* **46,** 1039–1049 CrossRef Medline
18. Ramsland, P. A., Willoughby, N., Trist, H. M., Farrugia, W., Hogarth, P. M., Fraser, J. D., and Wines, B. D. (2007) Structural basis for evasion of IgA immunity by *Staphylococcus aureus* revealed in the complex of SSL7 with Fc of human IgA1. *Proc. Natl. Acad. Sci. U.S.A.* **104,** 15051–15056 CrossRef Medline
19. Klychnikov, O. I., Shamorkina, T. M., Weeks, S. D., van Leeuwen, H. C., Corver, J., Drijfhout, J. W., van Veelen, P. A., Sluchanko, N. N., Strelkov, S. V., and Hensbergen, P. J. (2018) Discovery of a new Pro-Pro endopeptidase, PPEP-2, provides mechanistic insights into the differences in substrate specificity within the PPEP family. *J. Biol. Chem.* **293,** 11154–11165 CrossRef Medline
20. Parkin, G. (2004) Chemistry. Zinc-zinc bonds: a new frontier. *Science* **305,** 1117–1118 CrossRef Medline
21. Hakkim, V., and Subramanian, V. (2010) Role of second coordination sphere amino acid residues on the proton transfer mechanism of human carbonic anhydrase II (HCA II). *J. Phys. Chem. A* **114,** 7952–7959 CrossRef Medline
22. Shook, R. L., and Borovik, A. S. (2010) Role of the secondary coordination sphere in metal-mediated dioxygen activation. *Inorg Chem.* **49,** 3646–3660 CrossRef Medline
23. Christianson, D. W., and Cox, J. D. (1999) Catalysis by metal-activated hydroxide in zinc and manganese metalloenzymes. *Annu. Rev. Biochem.* **68,** 33–57 CrossRef Medline
24. Guo, F., and Martí-Rujas, J. (2016) Second sphere coordination of hybrid metal-organic materials: solid state reactivity. *Dalton Trans.* **45,** 13648–13662 CrossRef Medline
25. Fontecilla-Camps, J. C., Volbeda, A., Cavazza, C., and Nicolet, Y. (2007) Structure/function relationships of [NiFe]- and [FeFe]-hydrogenases. *Chem. Rev.* **107,** 4273–4303 CrossRef Medline
26. Zheng, L., Baumann, U., and Reymond, J. L. (2004) An efficient one-step site-directed and site-saturation mutagenesis protocol. *Nucleic Acids Res.* **32,** e115 CrossRef Medline
27. Pichlo, C., Montada, A. A., Schacherl, M., and Baumann, U. (2016) Production, crystallization and structure determination of *C. difficile* PPEP-1 via microseeding and zinc-SAD. *J. Vis. Exp.* e55022 CrossRef Medline
28. Pantoliano, M. W., Petrella, E. C., Kwasnoski, J. D., Lobanov, V. S., Myslik, J., Graf, E., Carver, T., Asel, E., Springer, B. A., Lane, P., and Salemme, F. R. (2001) High-density miniaturized thermal shift assays as a general strategy for drug discovery. *J. Biomol. Screen.* **6,** 429–440 CrossRef Medline
29. Carmona, A. K., Schwager, S. L., Juliano, M. A., Juliano, L., and Sturrock, E. D. (2006) A continuous fluorescence resonance energy transfer angiotensin I-converting enzyme assay. *Nat. Protoc.* **1,** 1971–1976 CrossRef Medline
30. Kabsch, W. (2010) XDS. *Acta Crystallogr. D Biol Crystallogr.* **66,** 125–132 CrossRef Medline
31. Afonine, P. V., Grosse-Kunstleve, R. W., Echols, N., Headd, J. J., Moriarty, N. W., Mustyakimov, M., Terwilliger, T. C., Urzhumtsev, A., Zwart, P. H., and Adams, P. D. (2012) Towards automated crystallographic structure refinement with phenix.refine. *Acta Crystallogr. D Biol. Crystallogr.* **68,** 352–367 CrossRef Medline
32. McCoy, A. J., Grosse-Kunstleve, R. W., Adams, P. D., Winn, M. D., Storoni, L. C., and Read, R. J. (2007) Phaser crystallographic software. *J. Appl Crystallogr.* **40,** 658–674 CrossRef Medline
33. Emsley, P., Lohkamp, B., Scott, W. G., and Cowtan, K. (2010) Features and development of Coot. *Acta Crystallogr. D Biol. Crystallogr.* **66,** 486–501 CrossRef Medline
34. Nguyen, B. D., Meng, X., Donovan, K. J., and Shaka, A. J. (2007) SOGGY: solvent-optimized double gradient spectroscopy for water suppression. A comparison with some existing techniques. *J. Magn. Reson.* **184,** 263–274 CrossRef Medline
35. Wüthrich, K. (1986) *NMR of Proteins and Nucleic Acids*, John Wiley and Sons, Hoboken, NJ
36. Keller, R. L. J. (2004) *The Computer Aided Resonance Assignment Tutorial*, Cantina Verlag, Goldau, Switzerland
37. Güntert, P. (2004) Automated NMR structure calculation with CYANA. *Methods Mol. Biol.* **278,** 353–378CrossRef Medline
38. DeLano, W. L. (2015) *The PyMOL Molecular Graphics System*, Version 1.8, Schrödinger, LLC, New York
39. Pettersen, E. F., Goddard, T. D., Huang, C. C., Couch, G. S., Greenblatt, D. M., Meng, E. C., and Ferrin, T. E. (2004) UCSF Chimera—a visualization system for exploratory research and analysis. *J. Comput. Chem.* **25,** 1605–1612 CrossRef Medline

Molecular determinants of the mechanism and substrate specificity of *Clostridium difficile* proline-proline endopeptidase-1

Christian Pichlo, Linda Juetten, Fabian Wojtalla, Magdalena Schacherl, Dolores Diaz and Ulrich Baumann

J. Biol. Chem. 2019, 294:11525-11535.
doi: 10.1074/jbc.RA119.009029 originally published online June 10, 2019